PHYSICAL REVIEW B **95**, 100502(R) (2017)

Nodeless multiband superconductivity in stoichiometric single-crystalline $CaKFe_4As_4$

Kyuil Cho,[1] A. Fente,[2] S. Teknowijoyo,[1] M. A. Tanatar,[1] K. R. Joshi,[1] N. M. Nusran,[1] T. Kong,[1] W. R. Meier,[1] U. Kaluarachchi,[1] I. Guillamón,[2] H. Suderow,[2] S. L. Bud'ko,[1] P. C. Canfield,[1] and R. Prozorov[1,*]

[1]*Ames Laboratory, Ames and Department of Physics & Astronomy, Iowa State University, Ames, Iowa 50011, USA*

[2]*Laboratorio de Bajas Temperaturas, Unidad Asociada UAM CSIC, Departamento de Física de la Materia Condensada, Instituto Nicolás Cabrera and Condensed Matter Physics Center (IFIMAC), Universidad Autónoma de Madrid, E-28049 Madrid, Spain*

(Received 20 June 2016; revised manuscript received 30 November 2016; published 8 March 2017)

Measurements of the London penetration depth $\Delta\lambda(T)$ and tunneling conductance in single crystals of the recently discovered stoichiometric iron-based superconductor $CaKFe_4As_4$ (CaK1144) show nodeless, two-effective-gap superconductivity with a larger gap of about 6–10 meV and a smaller gap of about 1–4 meV. Having a critical temperature $T_{c,\mathrm{onset}} \approx 35.8$ K, this material behaves similar to slightly overdoped $(Ba_{1-x}K_x)Fe_2As_2$ (e.g., $x = 0.54$, $T_c \approx 34$ K), a known multigap $s_\pm$ superconductor. We conclude that the superconducting behavior of stoichiometric CaK1144 demonstrates that two-gap $s_\pm$ superconductivity is an essential property of high-temperature superconductivity in iron-based superconductors, independent of the degree of substitutional disorder.

DOI: 10.1103/PhysRevB.95.100502

Iron-based superconductors (IBSs) are represented by a diverse group of different structural families all containing iron layers, which are believed to play the key role in superconductivity with the superconducting transition temperature T_c ranging from 2 to 56 K [1–3]. Most of these compounds contain fractional amounts of different ions forming superconducting domes as a function of the composition, resulting in complex phase diagrams and very rich physics [4–7]. The highest T_c is found at fractional compositions, which unavoidably have finite degrees of substitutional disorder. This represents a serious problem in understanding the pairing mechanism that is ultimately responsible for the high T_c's, because, in materials with anisotropic or sign-changing gaps, any disorder adds extra difficulty to quantify pair-breaking effects, in addition to non-spin-flip scattering [8,9]. Among the few stoichiometric IBSs, KFe_2As_2 ($T_c \approx 3.6$ K), LiFeAs ($T_c \approx 18$ K), LiFeP ($T_c \approx 5$ K) or LaFePO ($T_c \approx 6$ K), FeSe ($T_c \approx 9$ K in bulk crystals at ambient pressure) and FeS ($T_c \approx 5$ K), the recently discovered $CaKFe_4As_4$ (CaK1144) clearly stands out with a substantially higher value of $T_{c,\mathrm{onset}} \approx 35.8$ K and $H_{c2,c}(0) \approx 71$ T [10,11]. In addition, CaK1144 does not undergo structural or magnetic phase transitions [11]. Indeed, one could consider the 1:1 ratio of Ca and K simply as an ordered stoichiometric substitution of Ca for K at a 50% "doping" level. It is thus interesting to compare CaK1144 with hole-doped $Ba_{0.46}K_{0.54}Fe_2As_2$ which has a similar T_c of 34 K [12,13] but is randomly disordered on the single (Ba/K) site. Analysis of the thermodynamic data in CaK1144 crystals from the same batch as reported here estimates a mean free path of $\ell \approx 12.5$ nm, which is much larger than the coherence length of $\xi(0) \approx 2.15$ nm, placing this system in the clean limit [11].

In this Rapid Communication, the superconducting gap structure of $CaKFe_4As_4$ was studied by measuring the temperature-induced variation of the London penetration depth $\Delta\lambda(T)$ and the tunneling conductance at low temperatures, both of which probe the density of states (DOS) near the Fermi level E_F. The penetration depth shows saturation at low temperatures and the tunneling spectra exhibit a clear gap in DOS around E_F. In-depth data analysis leads to the conclusion that CaK1144 has two effective superconducting gaps. The smaller gap is in the range of 1–4 meV and the larger gap is 6–10 meV. The sizable spread is characteristic of superconductors showing different magnitudes of the superconducting order parameter over the Fermi surface. The larger ratio of the maximum to minimum gap values leads to an overall behavior quite similar to the overdoped $Ba_{1-x}K_xFe_2As_2$ (BaK122), $x = 0.54$, but different from the optimally doped BaK122, $x = 0.35$, where this ratio is about 2 [13,14].

Single crystals of $CaKFe_4As_4$ were synthesized by high-temperature solution growth out of FeAs flux (see Ref. [11] for details of the synthesis and comprehensive structural, thermodynamic, transport, magneto-optical, and spectroscopic characterization). Due to the complexity of the growth and potential for unwanted phases, each sample used in the present study was individually screened to be single phase. To this end, the in-plane four-probe resistivity was measured using a Quantum Design physical property measurement system (PPMS) in each sample with typical dimensions of approximately $2\times0.5\times0.02$ mm^3, and we checked that selected samples showed no extra features except for the superconducting transition [see Fig. 1(c)]. These samples had RRR $\equiv R(300\text{ K})/R(40\text{ K})$ of the order of RRR ≈ 15 (compared to RRR ≈ 7 of optimally doped BaK122 [12]).

The in-plane London penetration depth $\Delta\lambda(T)$ was measured using a self-oscillating tunnel-diode resonator (TDR) where the sample is subject to a small, 20 mOe, ac magnetic field, and the recorded resonant frequency shift from the value of the empty resonator is proportional to the sample's magnetic susceptibility, determined by λ and the sample shape. A detailed description of this technique can be found elsewhere [15–17].

For the scanning tunneling microscopy (STM) experiment, the sample was mounted onto a sample holder and a piece of brass was glued on top of it. At liquid helium temperature, the sample holder was moved toward a copper beam, lifting off the glued brass piece and leaving a freshly cleaved surface for tunneling [18,19]. Here, we present data taken

*Corresponding author: prozorov@ameslab.gov

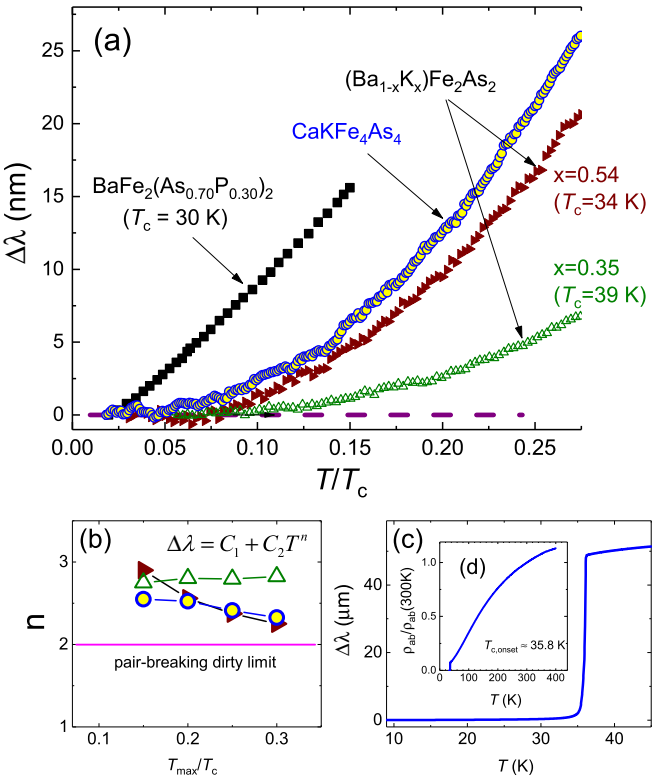

FIG. 1. (a) Variation of the London penetration depth $\Delta\lambda(T)$ in CaK1144 (solid circles) compared with other IBSs: $BaFe_2(As_{0.70}P_{0.30})_2$ (nodal gap, $T_c \approx 30$ K, solid squares) [26], $Ba_{0.65}K_{0.35}Fe_2As_2$ (no nodes, optimally doped, $T_c \approx 39$ K, open triangles), and $Ba_{0.46}K_{0.54}Fe_2As_2$ (no nodes, overdoped, $T_c \approx 34$ K, solid triangles) [13]. (b) Exponent n obtained from the power-law fit $\Delta\lambda = C_1 + C_2T^n$ as a function of the upper fit limit T_{max}/T_c. $n = 2$ represents the dirty-limit exponent for the sign-changing order parameters, such as d wave or $s_\pm$. Symbols are the same as in (a). (c) Full-temperature range variation of the in-plane London penetration depth $\Delta\lambda(T)$. (d) Normalized in-plane resistivity ρ_{ab}/ρ_{ab} (300 K) showing only the superconducting transition.

at 0.8 K. This corresponds to an energy resolution of about 70 μeV, determining roughly the interval between points in the tunneling conductance curves [18,20]. The measurements were conducted using a normal metal (gold) tip. The tunneling conductance was obtained by differentiating the I-V curves, as described in our previous works [21,22]. Flat surfaces for tunneling were found similar to other STM studies, for example, in BaK122 [23]. Note that we have measured hundreds of topographical images and millions of spectra and a detailed analysis will be published separately. We emphasize that the ubiquitous surface reconstruction discussed in STM work on the IBSs [23–25] is not found in $CaKFe_4As_4$. Instead, we observe atomically flat surfaces showing atomic size features that are separated by steps due to terminations of different crystallographical planes.

Figure 1(a) shows the low-temperature, $T/T_c \leqslant 0.3$, variation of London penetration depth $\Delta\lambda(T)$ in a single-crystal CaK1144 compared with three other IBSs with comparable T_c values: $BaFe_2(As_{0.70}P_{0.30})_2$ ($T_c \approx 30$ K), which exhibits a nodal gap [26] and two compositions of $(Ba_{1-x}K_x)Fe_2As_2$ with $x = 0.35$ (optimally doped, $T_c \approx 39$ K) with two isotropic gaps and $x = 0.54$ (overdoped, $T_c \approx 34$ K) that shows no nodes, but an increased angular anisotropy in at least one of the gaps [13]. Figure 1(c) shows a full-temperature range London penetration depth and normalized resistivity with a very sharp transition and no signatures of other phases or transitions.

To numerically characterize the low-temperature behavior, we look at the change in the penetration depth, which is directly related to the population of quasiparticles excited by thermal fluctuations, by using different upper limits of the fitting range T_{max}, thus effectively cutting off the quasiparticles with energies exceeding k_BT_{max} (note that throughout this Rapid Communication we use $k_B = 1$). First, in Fig. 1(b), we characterize the curvature of $\Delta\lambda(T)$ by using the power-law fitting $\Delta\lambda = C_1 + C_2(T/T_c)^n$. More details of the procedure are given in our previous study [13]. Offset and scaling coefficients C_1 and C_2 are not important, but the exponent n characterizes the curvature. In the case of a nodeless s_{++} gap, both the clean limit and nonmagnetic dirty limit for either single-band or multiband superconductivity $\Delta\lambda(T)$ is exponential at low temperatures and may be described by a large exponent, $n > 3$. The symmetry-imposed line nodes result in linear behavior, $n = 1$, and approach $n = 2$ in the dirty limit. Finally, in the case of sign changing, but fully gapped, $s_\pm$ pairing, the clean limit is exponential (experimentally large $n > 3$) and becomes quadratic, $n = 2$ in the dirty limit [13,27,28]. In CaK1144 we find the values of n clearly exceeding $n = 2$, ruling out a nodal gap. Moreover, the exponent n vs T_{max}/T_c follows almost exactly the behavior found in $Ba_{0.46}K_{0.54}Fe_2As_2$, which is also seen directly in Fig. 1(a). This behavior is consistent with the clean-limit $s_\pm$ pairing with two nodeless gaps [13].

To probe the spectroscopic gap in the density of states (which is generally different from the magnitude of the order parameter due to scattering [29]) we use the low-temperature Bardeen-Cooper-Schrieffer (BCS) asymptotic behavior expected for the penetration depth $\Delta\lambda = B_1 + B_2\sqrt{\pi\delta/2t}\exp(-\delta/t)$, where $t = T/T_c$ and B_1, B_2 and $\delta \equiv \Delta(0)/T_c$ are free parameters [17]. Figure 2 shows an example of a good-quality fitting with $T_{max}/T_c = 0.14$. By plotting δ versus the upper fit limit T_{max}/T_c, we expect a saturation when the fit becomes truly exponential, indicating a clean gap in the density of states. Indeed, the upper inset in Fig. 2 shows such a saturation below $T_{max}/T_c \approx 0.14$ at $\delta \approx 0.32 \approx 1$ meV. Simultaneously, the quality of the fit becomes better and saturates, indicated in the lower inset in Fig. 2, by the lowest value of the reduced $\chi^2 = \sum(f_{data} - f_{fit})^2/\mathrm{DOF}$, where the number of degrees of freedom, DOF, is the number of data points minus the number of free parameters.

In Fig. 3(a) we show a few representative tunneling conductance curves obtained within an area whose topography is shown in the insets of Fig. 3(a) and corresponding current versus bias voltage curves are shown in Fig. 3(b). We observe most often a negligible tunneling conductance at zero bias, indicating no states close to the Fermi level. We also observe well-developed quasiparticle peaks positioned at a bias voltage that changes depending on the surface plane. At some surfaces (blue and violet in Fig. 3), we observe a quasiparticle peak slightly above 10 mV and a kink at about 5 mV. At other

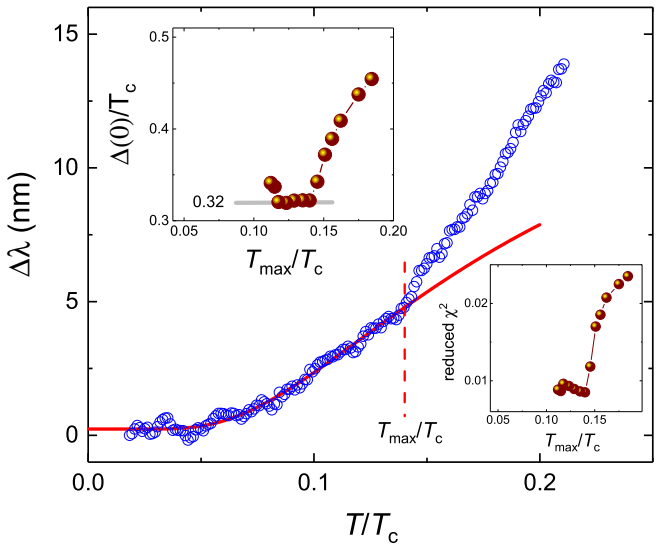

FIG. 2. A representative BCS fitting with Δ/T_c as a free fit parameter and fixed $T_{max}/T_c = 0.14$. Upper inset: Δ/T_c obtained from BCS fittings with different T_{max}/T_c. Lower inset: Reduced χ^2 vs T_{max}/T_c corresponding to the fitting results shown in the upper inset.

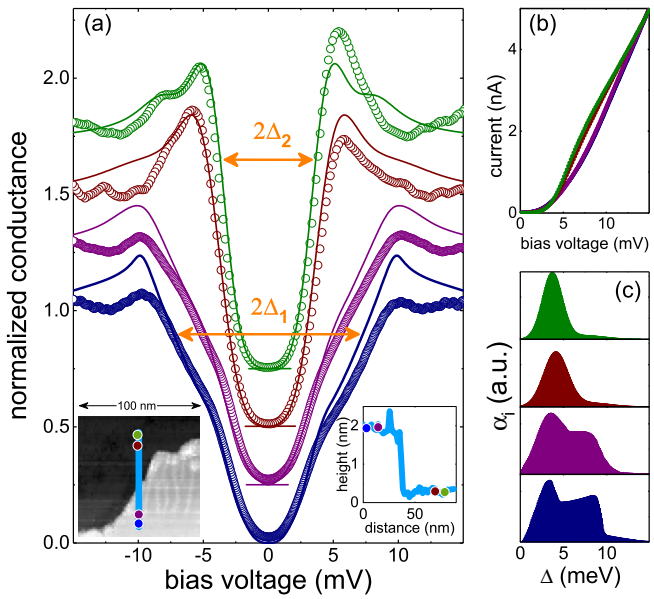

FIG. 3. (a) Tunneling conductance vs bias voltage curves measured at 800 mK (symbols) and corresponding fits to BCS theory (solid lines). The curves are shifted, and the zero conductance value is indicated by a horizontal line in each curve. The left inset shows the topography of the surface (image size is 100×100 nm^2) and the right inset shows a profile taken along the line shown in the left inset. Points along the line in the left inset provide the places where we took the curves of the main panel. The step shown in the profile is of the order of the unit cell c-axis parameter. Orange arrows mark the position of the two maxima in the distributions of Δ_i (see text). (b) Tunneling current vs bias voltage curves corresponding to the tunneling conductance curves shown in (a). (c) Distributions of the superconducting gap values (relative weight α_i and gap size Δ_i; see text) used to obtain the lines in (a). Colors of symbols in (a) are used to refer to corresponding curves in (b) and (c) and points in the insets of (a).

surfaces, we observe quasiparticle peaks at about 5 mV and shoulders somewhat below 10 mV (green and red in Fig. 3). This is a common observation in effective two-gap Fe-based superconductors (e.g., in BaK122 [23]). Different surface terminations lead to different matrix elements for the tunneling between the tip and the sample [30,31]. This, in turn, leads to spatially varying contributions to the density of states from different parts of the Fermi surface. When the gap is not uniquely defined, as in a simple s-wave BCS superconductor, the gap sizes involved in the tunneling process differ from the positions of the quasiparticle peaks in the bias voltage. To obtain the tunneling conductance and find the superconducting gap values, we have convoluted a density of states in the form $\alpha_i\,\mathrm{Re}(\frac{E}{\sqrt{E^2-\Delta_i^2}})$ with the derivative of the Fermi function to obtain the tunneling conductance [22,30,32,33]. The lines in Fig. 3(a) show the tunneling conductance calculated using the set of α_i and Δ_i shown in Fig. 3(c). The values of the superconducting gap are spread between about 1 and 10 meV. The α_i provides the relative weight in the tunneling conductance from the different gap values (see, e.g., Ref. [32] for similar results obtained in MgB_2). At all locations there are two peaks in the α_i. The height of each peak varies as a function of the tunneling plane. One peak is at ≈ 3 meV and another one at ≈ 8 meV. This corresponds, respectively, to $0.54\Delta(0)/T_c$ and $1.45\Delta(0)/T_c$ compared to $\Delta(0)/T_c = 1.76$ for the isotropic single-gap weak-coupling value. These values agree with the values inferred from the superfluid density, discussed next.

The superfluid density $\rho_s \equiv [\lambda(0)/\lambda(T)]^2$ can be obtained from $\lambda(T)$, provided we can estimate the absolute value of $\lambda(0)$. The TDR technique is suitable for the precision measurements of the changes in the penetration depth [34], but not the absolute value. We use two approaches to estimate $\lambda(0)$. First, the thermodynamic Rutgers relation is used to estimate the Ginzburg-Landau parameter $\kappa_{GL} = \lambda_{GL}/\xi_{GL}$ [11,35],

$$\kappa_{GL} = \sqrt{\frac{T_c}{8\pi\,\Delta C}}\left|\frac{\partial H_{c2,c}}{\partial T}\right|_{T_c}, \qquad (1)$$

where the jump of the specific heat erg/cm^3/K (using a molar volume of 115.4 cm^3/mol), the slope of the upper critical field (measured parallel to the c axis) at T_c, $dH_{c2,c}/dT = -4.4\times10^4$ Oe/K [11]. Equation (1) gives $\kappa_{GL} \approx 60$. As shown from the detailed analysis of $H_{c2}(T)$, due to a very short coherence length $\xi(0) = \sqrt{\phi_0/2\pi\,H_{c2}(0)} \approx 2.15$ nm [$H_{c2}(0) \approx 71$ T], CaK1144 appears to be in the clean limit [11]. Therefore, we can use the clean-limit relation $\kappa(0) = 1.206\kappa_{GL} = 68.7$ from which $\lambda(0) = \xi(0)\kappa(0) \approx 148$ nm. Alternatively, we can estimate Ginzburg-Landau $\xi_{GL} = \sqrt{\phi_0/2\pi\,T_c|\frac{\partial H_{c2}}{\partial T}|_{T_c}} \approx 1.5$ nm, which gives $\lambda_{GL} = \xi_{GL}\kappa_{GL} \approx 83$ nm. Therefore, $\lambda(0) = \sqrt{2}\lambda_{GL} \approx 118$ nm. These are quite close values resulting in a small variation of ρ_s at intermediate temperatures. For the fitting analysis of the superfluid density we use the average of these two values, $\lambda(0) = 133$ nm. The second determination of $\lambda(0)$ was made directly by measuring the field of the first vortex penetration on the sample edge

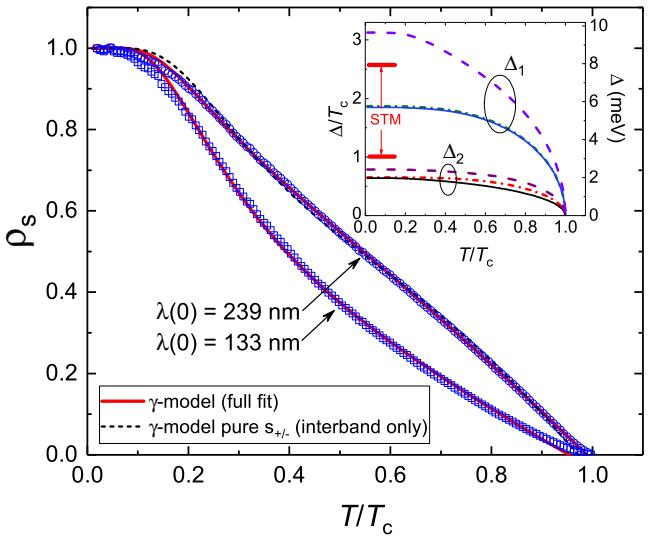

FIG. 4. Superfluid density ρ_s calculated with $\lambda(0) = 133$ nm (open squares) and $\lambda(0) = 239$ nm (open circles). Self-consistent γ-mode fits with all coupling parameters are shown as solid lines and the interband-only coupling fit is shown by the dashed line [for the $\lambda(0) = 239$ nm case]. The inset shows the temperature dependence of the two order parameters obtained from the fits in the main figure. Solid and dashed-dotted lines are for the all-parameter fits for the two values of $\lambda(0)$, respectively. The dashed lines are for the interband-only fit. The thick red lines mark the spread of the order parameter values determined from the STM measurements.

using recently developed sensitive and noninvasive optical magnetometry based on the NV centers in a diamond film [36]. The penetration field is converted to the lower critical field $H_{c1} = \phi_0(\ln\lambda/\xi + 0.5)/(4\pi\lambda^2)$ according to the theory developed by Brandt [37]. This direct experimental probe yields $\lambda(0) = 239$ nm. We used these two values as the lower and upper limits for $\lambda(0)$ to fit the results.

To further analyze multiband superconductivity, we fit the superfluid density $\rho_s(T)$ to a two-band γ model [38]. Importantly, the two values of the order parameter are calculated self-consistently at each temperature. The relative contribution γ from one band (and $1-\gamma$ from the second) is another fit parameter to obtain the total superfluid density. We obtained a very good agreement in the entire temperature range with the order parameters shown in the inset in Fig. 4. In the fit with $\lambda(0) = 239$ nm, we determined $\Delta_1(0)/T_c = 1.86$, $\Delta_2(0)/T_c = 0.64$, so that $\Delta_1(0)/\Delta_2(0) = 2.9$, which is almost a factor of 2 larger than that found for BaK122 [13]. In energy units, we obtain $\Delta_1(0) = 5.70$ meV and $\Delta_2(0) = 1.97$ meV. With $\lambda(0) = 133$ nm, despite the quite different magnitude, we obtained similar values of $\Delta_1(0)/T_c = 1.88$ and $\Delta_2(0)/T_c = 0.66$ or, in energy units, $\Delta_1(0) = 5.77$ meV and $\Delta_2(0) = 2.0$ meV. To explore all possibilities, we also used the interband-only $s_\pm$ model, used to analyze the H_{c2} data in CaK1144 [11]. The dashed line in Fig. 4 shows our attempt to fit $\rho_s(T)$ obtained with $\lambda(0) = 239$ nm to the interband-only (pure $s_\pm$) model. The result is quite reasonable, although not as good as the full fit described above. Here, we obtain two gap amplitudes 9.6 and 2.4 meV. As shown in the inset, these values are in a good agreement with 8 and 3 meV, as well as an overall gap size distribution between 1 and 10 meV, obtained from the STM experiments. Indeed, more precise calculations should take into account the gap anisotropies and the realistic three-dimensional electronic band structure. At present, this formidable task is beyond the scope of this work due to the lack of needed information.

In conclusion, precision measurements of the London penetration depth and low-temperature STM spectroscopy show unambiguously a fully gapped multiband superconductivity in single crystals of $CaKFe_4As_4$. An analysis with two effective gaps gives a small gap in the range of 1–4 meV and the large gap is 6–10 meV. The overall behavior is quite similar to slightly overdoped $Ba_{0.46}K_{0.54}Fe_2As_2$. Notably, while the overall spread of gap values (mostly given by the difference between the averages of the two ranges of gap sizes) is lower in the presence of substitutional disorder (i.e., in BaK122), the $s_\pm$ physics with two effective gaps is clearly present in stoichiometric and substituted systems with high T_c's.

We thank A. Gurevich, D. D. Johnson, A. Kaminski, V. G. Kogan, and Lin-Lin Wang for useful discussions. This work was supported by the US Department of Energy (DOE), Office of Science, Basic Energy Sciences, Materials Science and Engineering Division. Ames Laboratory is operated for the US DOE by Iowa State University under Contract DE-AC02-07CH11358. The work in Madrid was supported by the Spanish Ministry of Economy and Competitiveness (FIS2014-54498-R and MDM-2014-0377), by the Comunidad de Madrid through program Nanofrontmag-CM (S2013/MIT-2850) by Axa Research Fund, FP7-PEOPLE-2013-CIG 618321, and the European Research Council (Grant Agreement No. 679080). Madrid's group also acknowledges SEGAINVEX-UAM. W.R.M. was funded by the Gordon and Betty Moore Foundation's EPiQS Initiative through Grant GBMF4411.

[1] I. I. Mazin, Nature (London) **464**, 183 (2010).
[2] A. Chubukov, Annu. Rev. Condens. Matter Phys. **3**, 57 (2012).
[3] P. J. Hirschfeld, C. R. Phys. **17**, 197 (2016).
[4] D. C. Johnston, Adv. Phys. **59**, 803 (2010).
[5] J. Paglione and R. Greene, Nat. Phys. **6**, 645 (2010).
[6] P. C. Canfield and S. L. Bud'ko, Annu. Rev. Condens. Matter Phys. **1**, 27 (2010).
[7] G. R. Stewart, Rev. Mod. Phys. **83**, 1589 (2011).
[8] D. V. Efremov, M. M. Korshunov, O. V. Dolgov, A. A. Golubov, and P. J. Hirschfeld, Phys. Rev. B **84**, 180512 (2011).
[9] V. G. Kogan, Phys. Rev. B **80**, 214532 (2009).
[10] A. Iyo, K. Kawashima, T. Kinjo, T. Nishio, S. Ishida, H. Fujihisa, Y. Gotoh, K. Kihou, H. Eisaki, and Y. Yoshida, J. Am. Chem. Soc. **138**, 3410 (2016).
[11] W. R. Meier, T. Kong, U. S. Kaluarachchi, V. Taufour, N. H. Jo, G. Drachuck, A. E. Böhmer, S. M. Saunders, A. Sapkota,

A. Kreyssig, M. A. Tanatar, R. Prozorov, A. I. Goldman, Fedor F. Balakirev, Alex Gurevich, S. L. Bud'ko, and P. C. Canfield, Phys. Rev. B **94**, 064501 (2016).

[12] Y. Liu, M. A. Tanatar, W. E. Straszheim, B. Jensen, K. W. Dennis, R. W. McCallum, V. G. Kogan, R. Prozorov, and T. A. Lograsso, Phys. Rev. B **89**, 134504 (2014).

[13] K. Cho, M. Kończykowski, S. Teknowijoyo, M. A. Tanatar, Y. Liu, T. A. Lograsso, W. E. Straszheim, V. Mishra, S. Maiti, P. J. Hirschfeld, and R. Prozorov, Sci. Adv. **2**, e1600807 (2016).

[14] H. Kim, M. A. Tanatar, W. E. Straszheim, K. Cho, J. Murphy, N. Spyrison, J.-P. Reid, B. Shen, H.-H. Wen, R. M. Fernandes, and R. Prozorov, Phys. Rev. B **90**, 014517 (2014).

[15] R. Prozorov, R. W. Giannetta, A. Carrington, and F. M. Araujo-Moreira, Phys. Rev. B **62**, 115 (2000).

[16] R. Prozorov and R. W. Giannetta, Supercond. Sci. Technol. **19**, R41 (2006).

[17] R. Prozorov and V. G. Kogan, Rep. Prog. Phys. **74**, 124505 (2011).

[18] H. Suderow, I. Guillamon, and S. Vieira, Rev. Sci. Instrum. **82**, 033711 (2011).

[19] A. Fente, I. Guillamón, S. Ran, S. Vieira, H. Suderow, S. L. Bud'ko, and P. C. Canfield, J. Phys.: Conf. Ser. **568**, 022046 (2014).

[20] I. Guillamon, H. Suderow, S. Vieira, and P. Rodiere, Physica C **468**, 537 (2008).

[21] G. Rubio-Bollinger, H. Suderow, and S. Vieira, Phys. Rev. Lett. **86**, 5582 (2001).

[22] I. Guillamón, H. Suderow, S. Vieira, L. Cario, P. Diener, and P. Rodière, Phys. Rev. Lett. **101**, 166407 (2008).

[23] L. Shan, Y.-L. Wang, B. Shen, B. Zeng, Y. Huang, A. Li, D. Wang, H. Yang, C. Ren, Q.-H. Wang, S. H. Pan, and H.-H. Wen, Nat. Phys. **7**, 325 (2011).

[24] J. E. Hoffman, Rep. Prog. Phys. **74**, 124513 (2011).

[25] F. Massee, Y. Huang, R. Huisman, S. de Jong, J. B. Goedkoop, and M. S. Golden, Phys. Rev. B **79**, 220517 (2009).

[26] K. Hashimoto, K. Cho, T. Shibauchi, S. Kasahara, Y. Mizukami, R. Katsumata, Y. Tsuruhara, T. Terashima, H. Ikeda, M. A. Tanatar, H. Kitano, N. Salovich, R. W. Giannetta, P. Walmsley, A. Carrington, R. Prozorov, and Y. Matsuda, Science **336**, 1554 (2012).

[27] P. J. Hirschfeld and N. Goldenfeld, Phys. Rev. B **48**, 4219 (1993).

[28] V. G. Kogan, R. Prozorov, and V. Mishra, Phys. Rev. B **88**, 224508 (2013).

[29] V. G. Kogan and R. Prozorov, Phys. Rev. B **93**, 224515 (2016).

[30] H. Suderow, I. Guillamón, J. G. Rodrigo, and S. Vieira, Supercond. Sci. Technol. **27**, 063001 (2014).

[31] Ø. Fischer, M. Kugler, I. Maggio-Aprile, C. Berthod, and C. Renner, Rev. Mod. Phys. **79**, 353 (2007).

[32] P. Martinez-Samper, J. Rodrigo, G. Rubio-Bollinger, H. Suderow, S. Vieira, S. Lee, and S. Tajima, Physica C **385**, 233 (2003).

[33] J. Rodrigo and S. Vieira, Physica C **404**, 306 (2004).

[34] R. Prozorov, R. W. Giannetta, A. Carrington, P. Fournier, R. L. Greene, P. Guptasarma, D. G. Hinks, and A. R. Banks, Appl. Phys. Lett. **77**, 4202 (2000).

[35] H. Kim, V. G. Kogan, K. Cho, M. A. Tanatar, and R. Prozorov, Phys. Rev. B **87**, 214518 (2013).

[36] K. R. Joshi, N. M. Nusran, K. Cho, M. A. Tanatar, Y. Liu, T. A. Lograsso, S. L. Bud'ko, P. C. Canfield, and R. Prozorov (unpublished).

[37] E. H. Brandt, Phys. Rev. B **59**, 3369 (1999).

[38] V. G. Kogan, C. Martin, and R. Prozorov, Phys. Rev. B **80**, 014507 (2009).